

# Efficiency of proton-driven Weibel instability at thermalizing initially two-temperature astrophysical plasmas

Chuang Ren<sup>†‡§</sup>, Eric G. Blackman<sup>‡§</sup>, and Wen-fai Fong<sup>\*</sup>

<sup>†</sup>Department of Mechanical Engineering

<sup>‡</sup>Department of Physics and Astronomy

<sup>§</sup>Laboratory for Laser Energetics

University of Rochester, Rochester, NY 14627

<sup>\*</sup>Massachusetts Institute of Technology, Cambridge, MA 02139

May 25, 2019

## Abstract

Whether a faster-than-Coulomb collisionless mechanism equilibrates ion-electron plasmas with ions initially much hotter than electrons is a fundamental plasma physics question and important for understanding low-luminosity astrophysical accretion flows. Here we study whether Weibel instabilities driven by proton temperature anisotropy produce such a mechanism. From theory and particle-in-cell simulations, we find that although the Weibel instability amplifies magnetic fields much faster than the ion-electron collision rate, the ratio of the saturated magnetic energy to the initial ion energy scales as the fourth power of the electron to ion mass ratio for an initially unmagnetized plasma. The energy transferred to electrons is of order the saturated magnetic energy, and so the instability cannot induce a faster-than-Coulomb electron-ion equilibration. However, we suggest why the same instability for an initially modestly magnetized plasma would provide more efficient equilibration.

## 1 Introduction

Left alone, a two-temperature ion-electron plasma, with the ions at a higher temperature than the electrons, will eventually reach an equilibrium in which the two species reach the same temperature. Coulomb collisions provide a minimum equilibration rate, but whether a faster-than-Coulomb collisionless equilibration mechanism exists[1, 2, 3] for specific particle distributions and external conditions is both a fundamental question in plasma physics and important for understanding aspects of collisionless astrophysical phenomena such as radiatively inefficient accretion flows (RIAF) (e.g. Ref.[4]). Coulomb interactions are often assumed to be the only temperature equilibrator in this context.

The survival of a two-temperature plasma for a Coulomb equilibration time scale is particularly important for geometrically thick RIAFs of which advection dominated accretion flows (ADAFs) have been the archetype [5, 6, 7, 8]. In contrast to standard geometrically thin accretion discs (e.g. Ref.[9]), which can comfortably allow 10% of the binding energy of the accreting material to be converted into observable radiation around black holes, two-temperature accretion disks can in principle reduce the photon luminosity by many orders of magnitude for the same accretion rate. Indeed, the measured luminosities from the central engines of some nearby elliptical galaxies seem to be 3 to 5 orders of magnitude smaller than expected for their estimated accretion rates. Similar quiescent phases of accretion are also observed in some states of X-ray binaries. There is also X-ray evidence that in some supernova remnants the ion temperature is much higher than the electron temperature[10].

In the simplest ADAF model, the reduced luminosity results from three key features: (1) energy dissipated by viscosity is assumed to heat the protons, (2) only electrons radiate efficiently, and (3) if the only means of energy transfer between electrons and protons is Coulomb collisions, then a sufficiently collisionless plasma can be accreted onto the central object before the electrons receive enough energy to radiate the energy dissipated by the accretion. The gravitational binding energy of the accreting material is then retained as internal energy of the hot protons, and can be quiescently advected through the event horizon of a black hole. Since the associated internal energy per ion in an ADAF is of order  $m_p c^2 \sim 1\text{GeV}$ , the electrons are required to stay at a temperature much lower than the GeV ion temperature to ensure a low luminosity for a given accretion rate. ADAFs are thick discs because the thermal energy of the ions puffs up the disk. More general models of two temperature accretion involving outflows and convective feedback are also popular[11, 12, 13].

The assumption that heat transfer from the ions to the electrons occurs only by Coulomb collisions is necessary to ensure that a negligible fraction of the dissipated thermal energy is transferred to the electrons during the accretion infall time. This assumption has yet to be validated or invalidated (e.g. Ref.[14]). Doing so requires understanding the subtle plasma physics of the interactions among the ions, electrons, and electromagnetic fields. A systematic way to make progress is to test this assumption under a range of specific conditions. If the assumption is found to be violated for particular circumstances, then the associated instability and faster-than-Coulomb coupling would limit the applicability of two-temperature accretion paradigm. If the assumption is not violated for a particular set of conditions, this would not prove the viability of two-temperature plasmas in all circumstances and more circumstances would need to be tested. While the latter issue has discouraged some people from working on this problem, we think that a series of rigorous tests using different initial and boundary conditions is needed: Were the assumption to emerge as consistently valid for a range of different initial conditions, this would gradually solidify the robustness of the assumption for an increasingly wider range of viable conditions, and justify two-temperature accretion flows for those regimes tested.

In this spirit, we report one test of the assumption here, namely, whether the ion-electron energy transfer can be sped up via Weibel instabilities driven by an ion distribution anisotropy. For a real disk, the microphysics by which gravitational potential energy is converted to ion thermal energy is not fully understood, but presumably involves turbulence generated by a collisionless version [15] of a magneto-rotatioanl instability [16]. MHD turbulence is believed to anisotropically cascade [17] and it is likely in a collisionless system, the proton temperature may also incur anisotropies on small scales, transiently induced by the cascading turbulence. Similar to an anisotropic electron distribution, an anisotropic ion distribution can also drive a Weibel instability [18, 19] which amplifies fluctuating magnetic fields. How fast and how much energy the electrons then gain energy from the isotropizing protons via the amplified electromagnetic fields is the subject of our present work.

If energy transferred to electrons were a significant fraction of the initial ion energy, this would be a much more efficient process than Coulomb collisions for temperature equilibration because the ratio of maximum growth rate of the ion-driven Weibel instability  $\gamma_{max}$  (see Eq.6 below) to collisional ion-electron equilibration rate  $\nu_{eI}$  is

$$\frac{\gamma_{max}}{\nu_{eI}} = 7.2\alpha^{3/2} \frac{n\lambda_D^3}{\ln\Lambda} \sqrt{\frac{T_e}{Mc^2}} \left(1 + \frac{T_{Im}}{T_e M}\right)^{3/2}. \quad (1)$$

Here  $\alpha \geq 0$  is a measure of ion temperature anisotropy (defined more precisely in Sec.2),  $n$  the electron density,  $\lambda_D$  the Debye length,  $\ln\Lambda$  the Coulomb logarithm,  $T_e$  and  $T_I$  the electron and ion temperatures (multiplied by the Boltzmann constant, as throughout the paper), respectively,  $m$  and  $M$  the electron and ion masses, respectively, and  $c$  the velocity of light. For a proton-electron plasma with  $n = 10^{12} \text{ cm}^{-3}$ ,  $T_I = 10^{12} \text{ K}$ ,  $\alpha = 1$ , and  $T_e = T_{Im}/M$ ,  $\gamma_{max}/\nu_{eI} \sim 3 \times 10^7$ . This ratio is large, but the question is what fraction of the ion energy will be transferred to electron when the instability saturates?

Using theoretical analysis (Sec.2) and Particle-in-Cell (PIC) simulations (Sec.3), we show herein that the fraction of the ion energy transferred to the magnetic field via the Weibel instabilities scales as  $(m/M)^4$  for a single mode. For an initially unmagnetized plasma, this implies that the Weibel instabilities are insignificant to the ion-electron temperature equilibration process. However, in Sec.4 we discuss how the transferred energy fraction via the Weibel instabilities may dramatically increase for an initially more strongly magnetized plasma. We conclude in Sec. 4.

## 2 Growth and saturation of proton-driven Weibel instability

The linear growth rate  $\gamma$  of the Weibel instability has been derived for various anisotropic electron or ion distributions [18, 19]. For the ion driven case, Ref. [19] derived  $\gamma$  in the large growth rate and low plasma temperature limit for the “ion-pinch” case, where the electron distribution is an isotropic Maxwellian and the ion distribution consists of two bi-Maxwellian counter-streams [19]. Here we also study instability driven by the ions, but we

do not invoke any ion bulk streaming, and instead allow the instability to develop from ion temperature anisotropy alone. Also in contrast to [19], we focus on the the small growth rate, high ion temperature limit.

We assume that the electrons have an initially isotropic electron distribution given by

$$f_{e0}(\mathbf{v}, \mathbf{x}) = \frac{n}{(2\pi T_e/m)^{3/2}} \exp\left(-\frac{mv^2}{2T_e}\right), \quad (2)$$

while the ions take on a bi-Maxwellian distribution,

$$f_{I0}(\mathbf{v}, \mathbf{x}) = \frac{n}{(2\pi/M)^{3/2} T_{I\perp} \sqrt{T_{Ix}}} \exp\left(-\frac{Mv_\perp^2}{2T_{I\perp}}\right) \exp\left(-\frac{Mv_x^2}{2T_{Ix}}\right). \quad (3)$$

Here,  $n$  is the density of the electrons or the ions (singly charged ions are assumed for simplicity),  $T_e$  the electron temperature,  $v_\perp^2 = v_y^2 + v_z^2$ , and  $T_{Ix}$  and  $T_{I\perp} = T_{Iy} = T_{Iz}$  are the ion temperatures in the  $x$ -direction and in the directions perpendicular to  $x$  respectively. To study the linear stability of this system against the Weibel instability, we assume that the mode wave vector is in the  $x$ -direction,  $\mathbf{k} = k\hat{x}$ , and all perturbations have spatial and temporal dependence of  $\exp(ikx - i\omega t)$ . For simplicity, we do not consider any coupling between transverse and longitudinal modes[20, 21] and assume that the modes are transverse,  $\mathbf{E} = E_y\hat{y}$  and  $\mathbf{B} = B_z\hat{z}$ .

We follow the procedure of Ref. [19] in linearizing the Vlasov-Maxwell system of equations, which leads to the following dispersion relation,

$$\frac{k^2 c^2}{\omega^2} + \frac{\omega_{pe}^2}{\omega^2} [1 + \frac{1}{2} Z'(\xi_e)] + \frac{\omega_{pI}^2}{\omega^2} [1 + \frac{1}{2} Z'(\xi_I)] + \frac{\omega_{pI}^2}{2\omega^2} \alpha Z'(\xi_I) - 1 = 0. \quad (4)$$

Here  $\omega_{pe}^2 \equiv 4\pi q^2 n/m$  and  $\omega_{pI}^2 \equiv 4\pi q^2 n/M$  are the plasma frequency of each species,  $\xi_e \equiv \omega/(k\sqrt{2T_e/m})$  and  $\xi_I \equiv \omega/(k\sqrt{2T_{Ix}/M})$ ,  $Z'$  is the derivative of plasma dispersion function  $Z(\xi) \equiv \pi^{-1/2} \int_{-\infty}^{\infty} \exp(-\lambda^2)/(\lambda - \xi) d\lambda$  [22], and  $\alpha \equiv T_{I\perp}/T_{Ix} - 1$  represents the ion temperature anisotropy. Eq.4 can also be directly derived from Eq.(37) in Ref.[19] by removing bulk streaming from both species and assuming an isotropic electron distribution. Verified *a posteriori*, the growth rate for the ion-driven Weibel instability is small,  $|\omega|/kc \sim m/M$ . Therefore, we take the small argument limit,  $\xi \ll 1$ , for  $Z'(\xi), Z'(\xi) \approx -2 - 2i\sqrt{\pi}\xi$ , to further simplify the dispersion relation Eq.4. In this small growth rate limit, the displacement current term (the constant 1 on the left-hand side) can also be neglected. This leads to

$$\omega = i\sqrt{\frac{2}{\pi}} k \sqrt{\frac{T_e}{m}} \frac{m}{M} \left( \alpha - \frac{k^2 c^2}{\omega_{pI}^2} \right) (1 + \beta)^{-1}, \quad (5)$$

where  $\beta \equiv \sqrt{\frac{mT_e}{MT_{Ix}}}(1 + \alpha)$  is usually much less than 1 when  $T_e \leq T_{Ix}$  and  $m \ll M$ . Eq. (5) shows that the mode is unstable when  $\alpha > 0$  and  $k^2 c^2 < \omega_{pI}^2 \alpha$ . The maximum growth

rate is reached at  $k^*c = \omega_{pI}\sqrt{\alpha/3}$ , and is given by

$$\gamma_{max} = \sqrt{\frac{8}{27\pi}}\omega_{pI}\alpha^{3/2}\frac{m}{M}\sqrt{\frac{T_e}{mc^2}}(1+\beta)^{-1}. \quad (6)$$

Eq. (6) (with  $\beta \approx 0$ ) was used to derive Eq. (1).

The PIC simulations of [19] showed that the linear growth for a particular  $k$ -mode saturates when the magnetic field amplifies to  $B_s$  defined in the following expression

$$\gamma_k \sim \sqrt{kV_y q B_s / Mc}. \quad (7)$$

Here,  $\gamma_k$  is the linear growth rate for the mode  $k$  and  $V_y$  and  $M$  are the characteristic  $y$ -velocity and mass of the instability-driving species (the ions in our case).

Ref. [19] identifies the right-hand side of Eq.7 as the magnetic bounce frequency and concluded that the saturation results from particle-trapping. That the right-hand side of Eq.7 is the magnetic bounce frequency can be seen as follows. In a stationary periodic magnetic field,  $B_z = B_s \sin(kx)$ , there are two constants of motion for a particle of charge  $q$  and mass  $M$ , namely the canonical momentum  $P_y \equiv MV_y - (qB_s/kc) \cos(kx)$  and energy  $\epsilon \equiv M(V_x^2 + V_y^2)/2$ [23]. Thus, for a particle starting at  $x = x_0$  near the field null at  $x = 0$  ( $kx_0 \ll 1$ ) with initial speeds  $V_y(x_0) = V_0, V_x(x_0) = 0$ , we obtain

$$V_x^2(x) = -(2V_0qB_s/kMc)[\cos(kx) - \cos(kx_0)] - (qB_s/kMc)^2[\cos(kx) - \cos(kx_0)]^2. \quad (8)$$

Particles with  $qV_0 < 0$  subsequently move toward  $x = 0$  due to the magnetic force and are trapped. (Particles with  $qV_0 > 0$  move away from  $x = 0$  and are trapped near the neighboring null.) In the small field approximation (neglecting the  $B_s^2$ -term in Eq.8) the trapped particles near  $x = 0$  move between  $x = \pm x_0$  and the bounce period for these particles is

$$\begin{aligned} T &\approx \frac{2}{\sqrt{2|V_0q|B_s/kMc}} \int_{-x_0}^{x_0} \frac{dx}{\sqrt{\cos(kx) - \cos(kx_0)}} \\ &= \frac{4}{\sqrt{k|V_0q|B_s/Mc}} K\left(\sin \frac{kx_0}{2}\right), \end{aligned} \quad (9)$$

where  $K$  is the complete elliptical function of the first kind. Eq.9 shows that the right-hand side of Eq.7 scales as the magnetic bounce frequency. However, the bouncing and trapping of the particles are a part of the process creating the current perturbation that is necessary for the growth of the instability[24] and are present even in the linear growth stage. There was no physical explanation in [19] as to why an increase of bounce frequency leads to the saturation.

In fact, Eq.7 can be interpreted as a condition that the current perturbation from the particle bouncing and trapping reaches the maximum possible value in one  $e$ -folding time.

The Weibel instability is driven by the current created by and located near the nulls of the perturbed magnetic field. This can be seen most simply by assuming that initially all particles move only in the  $\pm y$ -direction with equal numbers moving at velocities  $-V_y$  and  $+V_y$ , resulting in zero  $j_y$  everywhere. When there is a perturbed magnetic field  $B_z$  with a  $k_x$ , because of the sign change of  $B_z$  near a certain null, the particles moving in one direction are trapped (in the  $x$ -direction) near the null and the particles moving in the opposite direction are deflected away from the null, creating a net current. Near the neighboring null, both the trapped and deflected particles move in reversed directions, resulting in a net current of an opposite sign. It is these alternating currents, represented by the  $\alpha$ -term in Eq. 4, that drive the instability. The net current density  $j_y$  created depends on how effectively the current of the opposite sign can be reduced by transverse deflection of particles away from the region of interest. The magnitude of the current can therefore be estimated from the deflected particle flux by

$$\frac{\partial j_y}{\partial t} \approx \frac{\partial}{\partial x} (j_M v_x), \quad (10)$$

where  $j_M = (1/2)n|qV_y|$  represents the maximum current density achievable, which would arise if all particles of one velocity sign leave the null region.

Due to magnetic deflection,  $\partial v_x / \partial t \approx \omega_c V_y$  where  $\omega_c = qB_z/Mc$  is the cyclotron frequency. Since  $\partial B_z / \partial x \approx kB_s$  near the null if  $B_s$  is the magnetic field amplitude, we obtain

$$\frac{\partial^2 j_y}{\partial t^2} \approx j_M \frac{qkB_s V_y}{Mc}. \quad (11)$$

Comparing Eq. (7) and Eq. (11), we can see that  $B_s$  is the field strength such that the current growth in one e-folding time reaches  $\sim j_M$ , after which the current can no longer increase and the mode saturates. This saturation mechanism also shows that  $q, V_y$ , and  $M$ , in Eq. (7) should be that of the locally anisotropic species (the ions in our case) since the net current creation from the trapping and bouncing would be zero for an isotropic distribution [24]. This identification of the responsive species could not be achieved solely based on the argument of magnetic trapping as the saturation mechanism since both species are trapped. This provides a physical interpretation of the result that Ref.[19] resolved only via PIC simulations.

From Eqs.(5) and (7) the mode with largest saturated magnetic field  $B_s$  has a mode number of  $k_m c = \omega_{pI} \sqrt{\alpha/5}$ , which is smaller than that of the fastest-growing mode,  $k^* c$ . Estimating the ratio of magnetic energy in this mode at saturation to the initial proton kinetic energy gives

$$\begin{aligned} \frac{E_B}{E_{kp}} &\equiv \frac{B_s^2/8\pi}{nT_{Ix}(3+2\alpha)} \\ &\sim 1.5 \times 10^{-2} \frac{\alpha^5}{3+2\alpha} \left(\frac{m}{M}\right)^4 \left(\frac{T_e/m}{T_{Ix}/M}\right)^2 (1+\beta)^{-4}. \end{aligned} \quad (12)$$

Because of the mass ratio factor, in a single mode  $E_B/E_{kp} \sim 2.6 \times 10^{-16}$  for an electron-proton plasma with  $\alpha = 1$  and  $T_e/m = T_{Ix}/M$ . This also approximates the total magnetic field energy if the spectrum at saturation is dominated by this mode. Because the magnetic energy is so small and because the only way for electrons to gain energy is through the magnetic energy, only a negligible fraction of the proton energy can be expected to be transferred to electrons when the Weibel instability saturates. The PIC simulations in Sec.3 will indeed show that the electron energy gain is on the same order of magnitude as the magnetic field energy gain. The upshot is that for an initially unmagnetized ion-electron plasma, the Weibel instability cannot generate electromagnetic fields of sufficient strength to energetically couple them to the protons.

### 3 PIC simulations

The saturation condition (7) was derived for a single mode, ignoring mode-mode interactions. To study how accurately Eq. (7) describes the saturation level when a range of unstable modes are present and whether Eq. (12) is a good estimation of the total magnetic field energy, we performed a series of PIC simulations with the fully explicit PIC code OSIRIS[25]. The simulations also provide a check on the theory of Weibel instabilities in the low growth rate regime[21] and include any relativistic effects neglected in the analysis. This regime is motivated by turbulent astrophysical plasmas of interest around black holes which are expected to have low to moderate temperature anisotropy (compared to Ref.[19]), moderately relativistic temperatures, and low growth rates. Previously, Davidson et al. performed PIC simulations to check the theory in the large anisotropy and large growth rate (large  $\xi$ ) regime[19].

In practice, PIC simulations of low growth rate instabilities are more difficult than those of a high growth rate. The number of particles used in a PIC simulation plasma is usually much smaller than that of the actual plasma it simulates. The resulting inflated fluctuations in the simulations, including the associated collisions, set a practical lower limit on the growth rate of a collisionless instability that can be reliably measured. Eqs.(6) and (12) show that an actual proton-electron mass ratio of  $M/m = 1836$  would produce too small a growth rate and too weak a magnetic field energy density to be practically measured in a simulation. We have therefore used  $M/m = 10 - 30$  in our simulations to check the ion mass scaling. Both electrons and ions were initially uniformly distributed in space, with a velocity distribution of the form  $\exp(-p_x^2/p_{tx}^2) \exp(-p_y^2/p_{ty}^2)$  where  $p_{x,y}$  is the normalized relativistic momentum components,  $p_{x,y} \equiv (v_{x,y}/c)/\sqrt{1 - v_x^2/c^2 - v_y^2/c^2}$ . The  $z$ -component of the velocity was kept to zero. For the electrons,  $p_{tx} = p_{ty} = 0.41$  were chosen, corresponding to  $\sqrt{T_e/mc^2} \simeq 0.38$  ( $T_e = 74$  keV) if we write  $T_e/mc^2 \approx p_{tx}^2/\sqrt{1 + p_{tx}^2 + p_{ty}^2}$ . For the ions,  $p_{tx} = 0.13$  and  $p_{ty} = 0.41$  were chosen, corresponding to  $\sqrt{T_{Ix}/Mc^2} \simeq 0.12$ ,  $\sqrt{T_{Iy}/Mc^2} \simeq 0.39$ , and  $\alpha = 9$ . (For protons, this corresponds

to  $T_{Ix} \simeq 15\text{MeV}$  and  $T_{Iy} \simeq 145\text{MeV}.$ ) The simulations used 1-1/2D (one full spatial dimension,  $x$ , and one half-dimension,  $y$ , where no spacial variation was allowed in  $y$ , and three velocity components but with  $V_z$  remaining zero throughout the runs) with a box size of  $240 c/\omega_{pe}$ . The cell size was  $\Delta x = 0.1c/\omega_{pe}$  and time step was  $\Delta t = 0.099/\omega_{pe}$ . To reduce fluctuations, 2500 to 18000 particles per cell were used for each species in typical runs. The total energy in these runs was conserved within  $10^{-6}$ .

Fig. 1 shows the Fourier spectrum of  $B_z$  at two different times,  $t_1 = 166\omega_{pe}^{-1}$  (in the linear growth stage) and  $t_2 = 305\omega_{pe}^{-1}$  (after saturation), for the  $M/m = 10$  case ( $\beta = 3$  and 2500 particles per cell were used.) During the linear growth stage, the growth rate  $\gamma$  for the  $k = 0.4\omega_{pe}/c$  was measured to be  $0.026\omega_{pe}$ , agreeing reasonably well with the analytical result of  $0.031\omega_{pe}$  obtained directly from Eq. (4). (Here,  $|\xi_I| \approx 0.45$  so the small  $\xi_I$ -expansion result of Eq. (5) is not accurate.) Following the same mode to saturation at  $t = 305/\omega_{pe}$ , the right hand side of Eq. (7) was found to be  $0.017\omega_{pe}$ , about 65% of the linear growth rate, consistent with Eq. (7) as a qualitative saturation criterion. This also implies that Eq. (12) is consistent only as an order-of-magnitude estimate. Fig. 1 also shows the shift of the dominant mode to lower  $k$  as the instability saturated, since  $k^*$  of the maximum growth mode decreases as  $\alpha$  decreases and also  $k_m$  of the highest saturation mode is smaller than  $k^*$ .

Fig. 2 shows the time evolution of the energy change in ions, electrons, and magnetic field ( $B_z$ -component), in units of the fraction of the initial ion energy. The curve for the magnetic energy is the total magnetic magnetic energy, with contributions integrated over the full range of  $k$ . This magnetic field energy reached  $\sim 1.8 \times 10^{-3}$  of the initial ion energy, which is of order  $1.3 \times 10^{-3}$  estimated from Eq. (12). The electron energy change at saturation was about  $3.4 \times 10^{-3}$ , significantly higher than the gain of  $1.8 \times 10^{-4}$  that corresponds to the gain from intrinsic collisions in the code: The latter baseline collisional gain was measured in a run with an isotropic ion distribution and found to depend linearly on  $t$  and inverse linearly on the number of particles per cell used. Therefore, the electron energy gain in the simulation of Fig. 2 was mainly due to collisionless processes as shown.

The ion mass scaling of (12) was checked by comparing the  $M/m = 10$  run with a run of  $M/m = 20$ . The saturated magnetic energy should scale as  $M^{-4}$  according to Eq. (12), and the time to reach saturation should scale as  $M^{3/2}$  (Eq. 6). Because the ion-electron collisional energy exchange rate in our simulations was found to scale as  $M^{-1}$ , as in a real plasma [26], it was necessary to increase the number of particles per cell to 18000 in the  $M/m = 20$  simulations to reduce the collisional energy exchange rate to below the collisionless instability-induced level. Fig. 3 shows the energy changes for the  $M/m = 20$  case. The saturated magnetic field energy reached at  $\sim 1.3 \times 10^{-4}$  of the initial ion energy, somewhat less, but to within order of magnitude of the  $5.3 \times 10^{-4}$  estimated from Eq. (12) (using  $\beta = 1.5$ ). The electron energy change at saturation was  $\sim 3.2 \times 10^{-4}$ , roughly scaling as  $M^{-3.4}$  when compared with the  $M/m = 10$  case. Overall, the PIC simulations support Eq. (12) as a rough estimation of the Weibel-induced energy exchange between the electrons and ions.

## 4 Summary and Future Directions

In summary, the linear growth rate of the Weibel instability driven by the proton temperature anisotropy has been calculated. A new interpretation has also been given for the formula estimating the saturation level of the magnetic field. These results show that the magnetic field energy at saturation scales as  $(m/M)^4$  and represents a negligible fraction of the initial proton energy. 1.5D PIC simulations with a reduced ion to electron mass ratio support scaling relations and also show that the electron energy gain from the proton anisotropy is comparable to the gain in magnetic field energy. Although in three dimensions one additional mode polarization is allowed and the number of unstable modes can double, we do not expect orders of magnitude change in the electron energy gain. From these analyses and simulations we conclude that the proton-driven Weibel instability will not provide an efficient faster-than-Coulomb electron-ion temperature equilibration mechanism in an initially unmagnetized two temperature plasma.

However, the situation may be dramatically different for an initially magnetized plasma in which electrons are confined to local magnetic field lines transversely. This case should be studied further. For modes with  $\mathbf{k}$  perpendicular to the equilibrium  $\mathbf{B}_0$ , the electrons would be practically immobile in the direction perpendicular to both  $\mathbf{B}_0$  and  $\mathbf{k}$ . As explained in Sec.2, the Weibel instability is driven by the current induced by the perturbed magnetic field  $B_z$ , represented by the term proportional to  $\alpha$  in Eq.4. However, additional currents with a different phase are also driven by the accompanied electric field  $E_y$ , which are represented by the second and third terms on the left of Eq.4. These currents are present even for an isotropic distribution and oppose mode growth. If the electrons were magnetized and could not respond to  $E_y$  to produce a current, the second term would not be present and the growth rate would be independent of  $m/M$ . This indicates that the required equilibrium magnetic field should be such that  $\omega_{ce} \gg \omega_{pI} \gg \omega_{cI}$  for this to happen, where  $\omega_{ce}$  and  $\omega_{cI}$  are the electron and ion cyclotron frequencies in the equilibrium magnetic field. In the case of the ion-driven (electricstatic) two-stream instability with magnetized electrons, the results were indeed found to be independent of the mass ratio[27]. If this also were true for the Weibel instability more generally, the saturated magnetic fields could store a significant fraction of the initial proton kinetic energy for an  $\alpha$  as low as 3 (Eq.12) and in principle could act as a mediator for faster-than-Coulomb electron-proton energy coupling, and could threaten the standard paradigm for two-temperature accretion flows.

## 5 Acknowledgments

C.R.'s work was supported by the US Department of Energy through grant No. DE-FC02-04ER54789 and the Junior Faculty Development Grant in Plasma Physics. E.B. acknowledges support from NSF grants AST-0406799, AST 00-98442, AST-0406823, NASA grant ATP04-0000-0016, and the Aspen Center for Physics.

## References

- [1] M.C. Begelman & T. Chiueh, *ApJ* **332**, 872 (1988).
- [2] E.G. Blackman, *MNRAS* **302**, 723 (1999).
- [3] E. Quataert & A. Gruzinov, *ApJ* **520**, 248 (1999).
- [4] E. Quataert, in *ASP Conf. Ser. 224: Probing the Physics of Active Galactic Nuclei*, edited by B. M. Peterson, R. W. Pogge, and R. S. Polidan, **224**, 71 (2001).
- [5] S. Ichimaru, *ApJ* **214**, 840 (1977).
- [6] M. J. Rees, E. S. Phinney, M. C. Begelman, R. D. Blandford, *Nature* **295**, 17 (1982).
- [7] R. Narayan and I. Yi, *ApJ* **452**, 710 (1995).
- [8] R. Narayan, R. Mahadevan, E. Quataert, in '*Theory of Black Hole Accretion Disks*', ed. Marek A. Abramowicz, Gunnlaugur Bjornsson, and James E. Pringle, Cambridge University Press, Cambridge, p.148 (1998).
- [9] N.I. Shakura & R.A. Sunyaev, 1973, *Astron.& Astrophys.*, **24**, 337
- [10] J. Vink, in '*Populations of high Energy in Galaxies*', Proceedings IAU Symposium No. 230. Edited by E. J. A. Meurs and G. Fabbiano, 2005.
- [11] E. Quataert, & R. Narayan, *ApJ* **520**, 298 (1999).
- [12] R.D. Blandford, & M.C. Begelman, *MNRAS*, **303**, L1 (1999).
- [13] R. Narayan, E. Quataert, I.V. Igumenshchev, & M.A. Abramowicz, *ApJ* **577**, 295 (2002).
- [14] V. I. Pariev and E. G. Blackman, *Baltic Astronomy* **14**, 265 (2005).
- [15] P. Sharma, G. W. Hammett, and E. Quataert, *ApJ* **596**, 1121 (2003).
- [16] S. A. Balbus and J. F. Hawley, *Reviews of Modern Physics* **70**, 1 (1998).
- [17] P. Goldreich and S. Sridhar, *ApJ* **485**, 680 (1997).
- [18] E. S. Weibel, *Phys. Rev. Lett.* **2**, 83 (1959).
- [19] R. C. Davidson, D. A. Hammer, I. Haber, and C. E. Wagner, *Phys. Fluids* **15**, 317 (1972).
- [20] C. Ren et al., *Phys. Rev. Lett.* **93**, 185004.

- [21] M. Tzoufras et al., Phys. Rev. Lett. **96**, 105002 (2006).
- [22] B. D. Fried and S. D. Conte, 'The Plasma Dispersion Function,' Academic Press, New York, 1961.
- [23] R. L. Morse and C. W. Nielson, Phys. Fluids **14**, 830 (1971).
- [24] B. D. Fried, Phys. Fluids **2**, 337 (1959).
- [25] R. G. Hemker et al., Proceedings of the 1999 Particle Accelerator Conference, edited by A. Luccio and W. Mackay (IEEE, Piscataway, NJ, 1999), Vol. 5, p. 3672; R. Fonseca et al., Lecture Notes in Computer Science (Springer, Heidelberg, 2002), Vol. 2331, p. 342.
- [26] B. A. Trubnikov, in *Review of Plasma Physics*, Vol. 1, Consultants Bureau, New York (1965).
- [27] K. Papadopoulos, R. C. Davidson, J. M. Dawson, I. Haber, D. A. Hammer, N. A. Krall, and R. Shanny, Phys. Fluids **14**, 849 (1971).

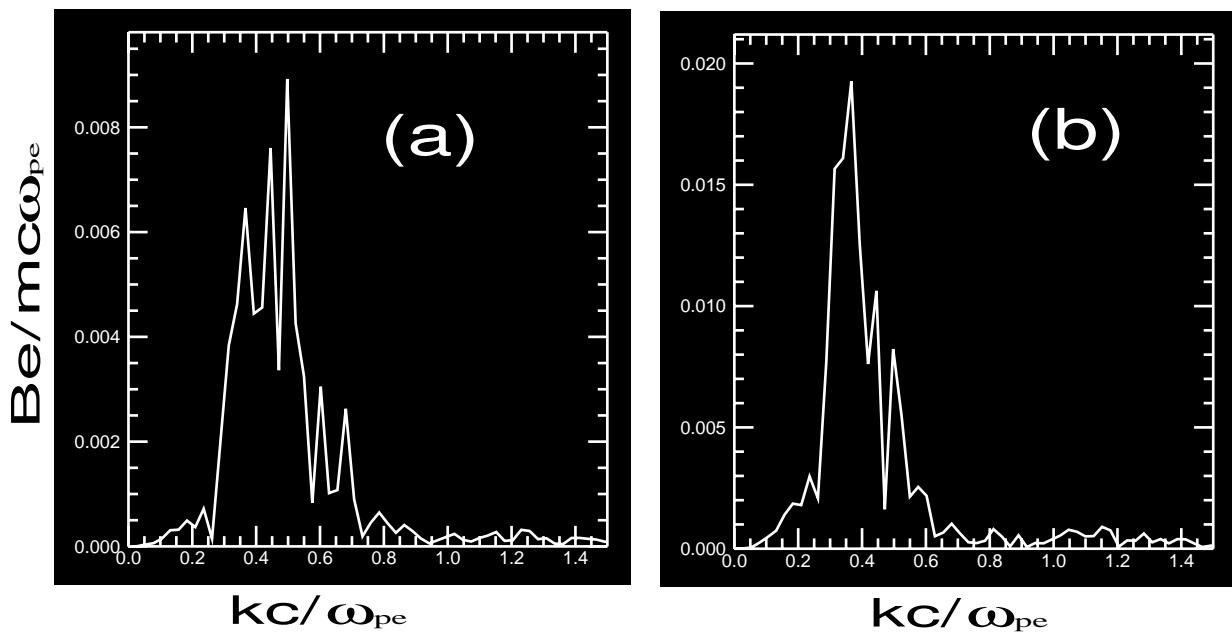
Figure 1: Fourier spectrum of  $B_z$  at two different times,  $t_1 = 166\omega_{pe}^{-1}$  (a) and  $t_2 = 305\omega_{pe}^{-1}$  (b), for the  $M/m = 10$  case.

Figure 2: The energy change of the ions, electrons, and magnetic field, in unit of the fraction of the initial ion energy, for the  $M/m = 10$  case.

Figure 3: The energy change of the ions, electrons, and magnetic field, in unit of the fraction of the initial ion energy, for the  $M/m = 20$  case.

This figure "fig2-m=10.jpg" is available in "jpg" format from:

<http://arxiv.org/ps/astro-ph/0608041v1>



This figure "fig3-m=20.jpg" is available in "jpg" format from:

<http://arxiv.org/ps/astro-ph/0608041v1>